pH Dependence of γ-Aminobutyric Acid Iontronic Transport

Maria Seitanidou, Juan Felipe Franco Gonzalez, Theresia Arbring Sjöström, Igor Zozoulenko, Magnus Berggren and Daniel T. Simon

Seitanidou, M., Franco Gonzalez, J. F., Arbring Sjöström, T., Zozoulenko, I., Berggren, M., Simon, D. T., (2017), pH Dependence of γ-Aminobutyric Acid Iontronic Transport, *Journal of Physical Chemistry B*, 121(30), 7284-7289. https://dx.doi.org/10.1021/acs.jpcb.7b05218

Original publication available at:
https://dx.doi.org/10.1021/acs.jpcb.7b05218

pH–Dependence of Gamma-Aminobutyric Acid Iontronic Transport

Maria Seitanidou[1], Juan Felipe Franco-Gonzalez[1], Theresia Arbring Sjöström[1], Igor Zozoulenko[1], Magnus Berggren[1], Daniel T. Simon[1]*

1. Laboratory of Organic Electronics, Department of Science and Technology, Linköping University, 60174 Norrköping, Sweden.

* Corresponding author: daniel.simon@liu.se

ABSTRACT

The organic electronic ion pump (OEIP) has been developed as an "iontronic" tool for delivery of biological signaling compounds. OEIPs rely on electrophoretically "pumping" charged compounds, either at neutral or shifted pH, through an ion-selective channel. Significant shifts in pH lead to an abundance of H^+ or OH^-, which are delivered along with the intended substance. While this method has been used to transport various neurotransmitters, the role of pH has not been explored. Here we present an investigation of the role of pH on OEIP transport efficiency using the neurotransmitter γ-aminobutyric acid (GABA) as the model cationic delivery substance. GABA transport is evaluated at various pHs using electrical and chemical characterization, and compared to molecular dynamics simulations, all of which agree that pH 3 is ideal for GABA transport. These results demonstrate a useful method for optimizing transport of other substances and thus broadening OEIP applications.

INTRODUCTION

Organic bioelectronics has emerged in recent decades as a technological solution to a variety of diagnostic and therapeutic applications. For example, biosensing, electrophysiological recording, and drug delivery systems have been demonstrated which were previously difficult or impossible to achieve with pharmaceutical or traditional electronic techniques.[1] Organic bioelectronics are made possible by the combined electronic and ionic properties of organic

electronics, and one area where these properties have been extensively leveraged is in the study – and ultimately treatment – of neurological disorders.[2–5] So called "iontronics" are a sub-discipline of organic bioelectronics, focusing on organic electronic components and circuits using metal ions, and even charged neurotransmitters, as the charger carrier. The fundamental component of iontronics is the organic electronic ion pump (OEIP), an electrophoretic drug delivery device that can be considered an iontronic resistor.[5–7] OEIPs are based on transporting, or "pumping", charged species through cation- or anion-exchange membranes (CEMs or AEMs), resulting in high spatiotemporal delivery resolution, high dosage precision (in principle, one electron corresponds to one delivered ion), and unlike analogous microfluidics-based techniques, no liquid flow. OEIP technology has been demonstrated to trigger cell signaling *in vitro*[8,9], to control epileptiform activity in brain slice models[3,10], to effect sensory function *in vivo*[7], as therapy for a pain in awake animals[5], and even to modulate plant growth via hormone delivery[11]. Additional iontronic components and systems, based on the OEIP concept, have also been developed: ion bipolar membrane diodes (IBMDs)[12], ion diode rectifier circuits[13], ion bipolar junction transistors (IBJTs) and logic circuits[14,15], and matrix-addressable high-speed drug delivery systems[16].

These various OEIP-based technologies are all based on transport of charged species through CEMs or AEMs. CEMs are characterized by a high concentration of fixed negative charge, and the permselectivity holds if the ionic concentrations in the adjacent electrolytes are lower than the CEM's fixed-charge concentration, *i.e.*, Donnan exclusion.[17] This permselectivity to cations does not discriminate specific cationic species, and the relative contribution to the overall ion flux through the CEM will be dependent on the various species' mobility through the membrane (or equivalently, their diffusion coefficients). The diffusion-coefficient-dependent relative transport becomes problematic since any H^+ present in the source solution have a higher diffusion coefficient than positively charged biomolecules like neurotransmitters. Thus, there

is a risk that cation transport through the CEM is dominated by H^+, and equivalently that anion transport through an AEM is dominated by OH^-.

To broaden the assortment of biologically relevant substances that can be effectively transported through OEIPs, the pH in the source reservoir can be shifted above or below the delivery substance's isoelectric point by adding OH^- or H^+, respectively.[5,7,10] However, this method results in the problem stated above: by adding H^+ to the source solution to achieve a cationic ("pumpable") form of, *e.g.*, a neurotransmitter, the delivery flux becomes an ill-defined mixture of the neurotransmitter and H^+. Additionally, while the relationship between pH and the charge state of the delivery molecule is known, the exact relationship between source pH and OEIP delivery efficiency is not well understood. Thus, many of the previous bioelectronics demonstrations of OEIP technology have required positive controls using H^+-only delivery, and could not report a precise dosage rate.[3,5,7,10]

In this study, we address this issue by presenting a systematic investigation of the effects of varying the pH on OEIP-based delivery. We use the neurotransmitter γ-aminobutyric acid (GABA) as the model delivery substance (as a cation through a CEM), as it is one of the primary neurotransmitters in the central nervous system and has been used in a variety of previous OEIP demonstrations.[3,5,7,10] The polyanion Poly(4-styrenesulfonic acid-co-maleic acid (PSS-co-MA) cross-linked with the polyalcohol polyethylene gylcole (PEG) was chosen as the model CEM material, where PSS is the primary ion exchange group. PSS is also the dopant species in poly(3,4-ethylenedioxythiophene) polystyrene sulfonate (PEDOT:PSS), the current material-of-choice for a variety of organic bioelectronics applications.[1,18] Understanding the precise relationship between pH and GABA delivery can provide clarification for previous OEIP demonstrations, and provide insight into future bio-iontronic applications.

METHODS

OEIP Fabrication

Glass substrates were cleaned and rinsed in acetone and deionized water. The adhesion promoter 3-glycidoxypropyltrimethoxysilane (GOPS; Sigma-Aldrich; 1 ml) was added to ethanol (47.5 ml), water (2.5 ml), and acetic acid (50 µl) and mixed for 15 min. Then the glass substrates were activated via O2 plasma for 30 s (Advanced Vacuum Reactive Ion Etch, O2 400 sccm, 250 W) just before they were soaked in the GOPS solution for 1 min. The adhesion layer was finalized by a quick rinse in ethanol and a baking step at 110 °C for 15 min. The polyanion Poly(4-styrenesulfonic acid-*co*-maleic acid) (PSS-co-MA, Sigma-Aldrich, M_w ~20000, transformed from Na^+ form to H^+ form by dialysis, 4 wt%) was mixed with polyethylene gylcole (PEG, M_w ~400, 1.5 wt%)) in water:1-propanol 1:1 for cross-linking and then deposited by spin-coating at 1500 rpm to obtain a thickness of approximately 300 nm. The substrates were then baked at 110 °C for at least 1 hour. A thin layer of poly(methyl methacrylate) (PMMA; Sigma-Aldrich; Mw ~ 12000, 4 mg/ml in diethyl carbonate) was deposited on top of the PSS-co-MA/PEG film for improved adhesion of the photoresist. The photoresist Shipley S1813 G2 was then deposited, exposed (MA6-BA6 Süss Mask Aligner), and developed in Microposit MF319. Reactive ion etching [O_2, 100 standard cubic centimeter per minute (SCCM); CF_4, 200 SCCM, 150 W, 90 s] was used to obtain the patterned PSS-co-MA/PEG CEM channels (3 mm long, 450 µm wide). The remaining photoresist and PMMA were removed using acetone. Substrates were then soaked in 0.1 M NaCl(aq) for 5 min to ensure that Na^+ remained the dominant counterion before encapsulation with SU-8 3010 (MicroChem). SU-8 was spin-coated at 3000 rpm, soft-baked for 10 min, including a ramping from 65 to 95 °C, exposed, post exposure baked for 1 min at 95 °C, and developed in Mr-Dev 600, resulting in approximately 10 µm thick films. The SU-8 pattern defined hydrophobic confinements for the two electrolytes: source and target. A final bake was carried out at 110°C for at least 15 min. Carbon contacts (DuPont 7082) were painted at the edge of each electrolyte

opening in the SU-8 (followed by 15 min bake at 100 °C), and Ag/AgCl paste (GWENT) was painted on top of the carbon to ensure an electrochemically stable electrode (followed by 10 min bake at 100 °C).

Electrical and Chemical Characterization

Electrical characterization was performed using a Keithley 2602 SourceMeter with custom LabVIEW software. 10 V was applied to the source electrode, with the target system grounded. pH in the target reservoir was measured using an Orion Star A211 pH Meter (Thermo-Scientific). Several samples were collected in this way from the different devices, and thereafter, chemical quantification of GABA was performed via ELISA assay (LDN/ BA E-2500) measured on a BioTek Synergy H1m plate reader, following the assay supplier's protocol. Differences between devices and experimental runs were negligible. The efficiency of the device was estimated by calculating the amount of delivered GABA divided by the number of electrons passed through the circuit, and averaging the values obtained from the various experiments.

Molecular Dynamics Simulations

Molecular dynamics were performed using a cubic box with 60 GABA molecules solvated by water at around 0.1 M, plus *n*-propanol, PEG (n=8), and PSS (n=60) at concentrations 8.6 wt%, 0.8 wt%, and 1.78 wt%, respectively. Partial charges per atom in each molecule were calculated using the ab initio density functional theory (DFT) functional WB97XRD[19] with the 6-31+g(d)[20] basis set, and fit to the electrostatic potential (ESP)[21] as implemented in the Gaussian suite[22] (Figure S1). The molecules were built using the topology described by the General AMBER Force Field (GAFF)[23] and a model SPC/E[24] for water. The system was then minimized and equilibrated for a 20 ns production run by an *NPT* assemble with a barostat and thermostat as Nose-Hoover[25–27] (at 1 atm and 293.15 K) using the LAMMPS suite[28].

Calculation of Diffusion Coefficient

Mean Square Displacement (MSD) of the molecules *A* from a set of initial positions was calculated according to the following Equation 1 (Stokes-Einstein relation[29]) and implemented in the GROMACS package[30]:

$$\lim_{t\to\infty}\langle\|\vec{r}_A(t)-\vec{r}_A(t_0)\|^2\rangle = 6D_A t \qquad \text{(Eqn. 1)}$$

where, angle brackets denote an ensemble average over the sampled molecules *A*; $\overrightarrow{r_A}$ corresponds to the coordinates of the center of mass of molecule *A* at initial time t_0 and time *t*; and D_A is the diffusion coefficient of molecule *A*. This provides an easy way to compute *D*. The diffusion constant is calculated by least squares fitting a straight line through the MSD(t) from 19 ns to 20 ns of the production MD run. The slop of the rectilinear line corresponds to *D*, as shown in Eqn. 1. An error estimate is given, which is the difference of the diffusion coefficients obtained from fits over the two halves of the fit interval and averaged over all cationic GABA molecules.

RESULTS AND DISCUSSION

PSS-based OEIPs were fabricated on glass substrates with 3 mm long, 450 µm wide CEM channels (Figure 1). The relationship between pH and performance was first determined using electrical characterization. The source reservoir was loaded with 0.1 M GABA (aq) and pH-adjusted by addition of HCl (in the pH range 2-6), and a constant voltage of 10 V was applied (Figure 2a). After several hundred seconds, the current stabilized, dependent on the pH and thus the $[GABA^+]_s$:$[H^+]$ ratio, where $[GABA^+]_s$ is the GABA concentration in the source (Figure 2a (left curve), Figure 2b). At this point (900 s), the source GABA solution was exchanged for HCl(aq) at the same pH. Figure 2a illustrates that the time to steady current and the stable current level are dependent on the relative size and abundance of the transported ions. From the fabrication stage, Na^+ is likely to be the dominant counterion in the PSS-co-MA/PEG channel.

Thus, the rise times observed in the Figure 2b indicate a complex exchange of Na^+ for a mix of (the higher mobility) H^+ and (lower mobility) $GABA^+$, with faster rise times generally observed for higher $[H^+]$ in the source solution. The rise times after the switch to HCl(aq) (after 900 s) reflect a simpler exchange of H^+ for any remaining $GABA^+$ in the channel. The steady-state currents (around 1800 s) rise with decreasing pH, with a significant jump in current for pH 2. This pH is close to the pKa of PSS (pKa 1)[31–33], indicating that proton-conducting state may be arising. Taking the stable currents at each pH for the GABA and HCl solutions (*i.e.*, at 900 s and 1800 s) and converting to ionic conductivity using the PSS channel geometry, we can visualize the conductivity as a function of pH (Figure 2c).

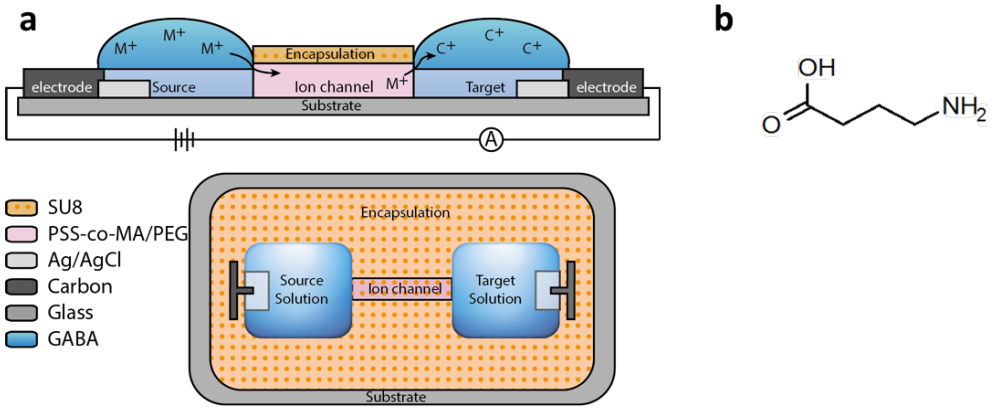

Figure 1. (a) Schematic illustration of the organic electronic ion pump (OEIP); (b) GABA structure.

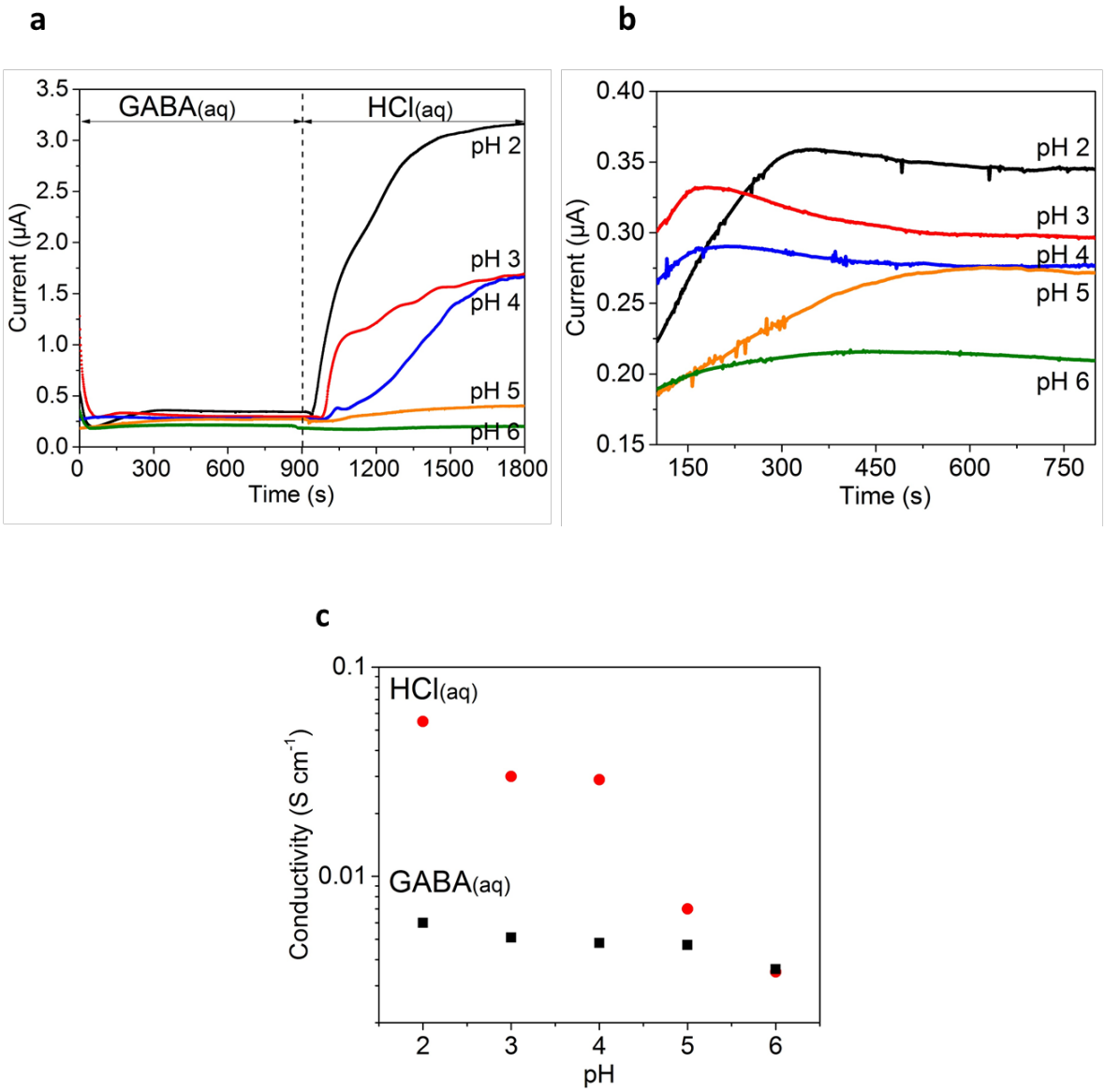

Figure 2. Electrical characterization. (a) Ion pump current vs time for various pH of source electrolyte, for source electrolyte GABA(aq) (t < 900 s) and HCl(aq) (t > 900 s) for V_{appl} = 10 V; (b) Zoom of curve in part a for source electrolyte GABA; (c) Dependence of ionic conductivity on pH for GABA(aq) (black squares) and HCl(aq) (red circles) source electrolytes as defined from the steady state current in curve a using Ohm's law and taking into account the geometry of the channel.

To ascertain the efficiency of OEIPs, chemical quantification of delivery must be performed. The efficiency of OEIP transport is defined as the ratio between the number of intended molecules (GABA) transported into the target reservoir (chemically quantified by sampling the electrolyte after delivery) to the number of electrons recorded in the driving circuit, *i.e.*, the integrated current. For example, 100% efficiency would correspond to one GABA molecule per electron, and 20% efficiency would indicate that 80% of the ionic current was due to the transport of some other species, such as H^+. GABA(aq) source solutions were pH-adjusted by addition of HCl(aq)(1M), resulting in changes in $[GABA^+]_s$ related to both dilution and protonation/pKa (Figure S2 and Table S1). $[GABA]_t$ (concentration in the target solution/reservoir) was determined via a specific ELISA assay. With both $[GABA]_s$ and $[GABA]_t$ quantified at each source pH value, we could compare the effective combined ionic conductivity (for all transported species) vs source pH (Figure 3a). Although, the theoretical $[GABA^+]_s$ is higher at pH 2 (Figure S2), it is decreased by half after dilution with HCl(aq). At this pH, the higher conductivity is likely due entirely to H^+ transport. As expected, the transport efficiencies at pH 3 and higher decrease with decreasing $[GABA^+]_s$ in the source electrolyte (Figure S2). Our results indicate that pH 3 gives the highest transport efficiency for $GABA^+$ (Figure 3b).

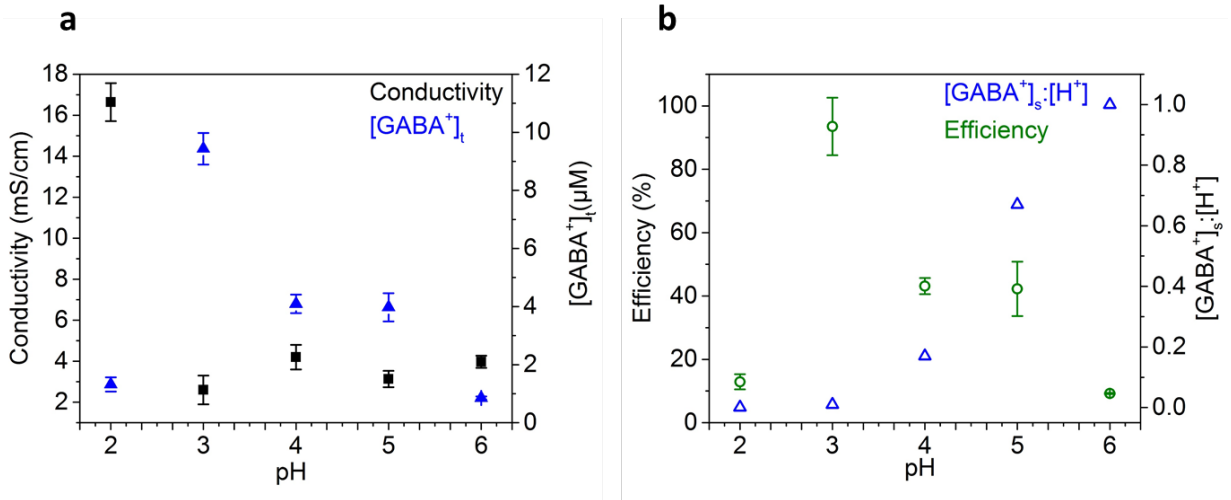

Figure 3. Chemical characterization. (a) Dependence of ionic conductivity for I_{appl} = 200 nA and delivered $[GABA^+]_t$ on various pH of source GABA(aq) electrolyte; (b) Dependence of efficiency of GABA delivery and $[GABA^+]_s$:$[H^+]$ ratio on pH of source GABA electrolyte. Efficiency is defined as the number of GABA molecules transported into the target reservoir divided by the number of electrons recorded in the driving circuit.

We hypothesize that the high efficiency at pH 3 is due to an optimal $[GABA^+]_s$:$[H^+]$ ratio maximizing positively charged GABA while minimizing available H^+ for co-transport, as well as an optimal GABA configuration. It has been reported that the zwitterionic GABA molecule exhibits pH-dependent conformation changes, passing from an extended structure to a tighter "folded" structure with the lowest free energy[34]. Classical molecular dynamics (MD) simulations were performed to investigate the role of GABA's pH-dependent conformational changes and subsequent changes in transport characteristics. Sixty GABA molecules were modeled at approx. 0.1 M in water, together with n-propanol, PEG, and PSS. Three scenarios were modeled: (*i*) 100 % cationic GABA; (*ii*) mixture of cationic (80 %) and zwitterionic (20 %) GABA; and (*iii*) mixture of 50 % of both GABA species. They were respectively considered in the proper proportion to achieve pH values of about of 1, 3, and 4. Figure 4a shows the conformational structures of cationic GABA in the three scenarios. The cationic species are mostly folded or cyclic, but the simulation indicates a more globular conformation at pH 3 where the ammonium moiety (green) is more closely aligned to the carbonyl group. The radius of the sphere containing the structure (radius of gyration) does not show significant variation, with changes only on the order of 5 %. However, the model does predict $GABA^+$ at pH 3 to have a smaller overall structure, and therefore a potentially higher mobility/diffusion coefficient. In addition, the globular conformation at pH 3 results from a Coulomb interaction between the ammonium cation and the carboxyl group of GABA, whereas at other pHs, the

ammonium cations may be free to interact with negative sulfonate groups on the PSS chain, leading to effective loss of mobility.

To investigate further, the diffusion coefficient (*D*) was calculated for each pH (Figure 4b). The MD results verify that the maximum diffusion coefficient corresponds to the smallest globular conformation of GABA at pH 3. The diffusion coefficient and electrophoretic mobilities satisfy the Nernst-Einstein relation:

$$\Lambda^0_{m,i} = z_i^2 D_i \left(\frac{F^2}{RT}\right)^{35} \quad \text{(Eqn.2)}$$

where, $\Lambda^0_{m,i}$ is the molar limiting conductivity, F is the Faraday constant, R is the gas constant, T is the thermodynamic temperature and D is the diffusion coefficient for any given ion i. So the higher diffusion coefficient indicated a higher mobility at pH 3. Thus, GABA at pH 3 would account for a larger proportion of the cation flux through the OEIP. Although the modelled variation in *D* is too small to account for up to 10x changes in delivery efficiency (Figure 4b), these MD results are the first evidence to indicate a significant effect around pH 3.

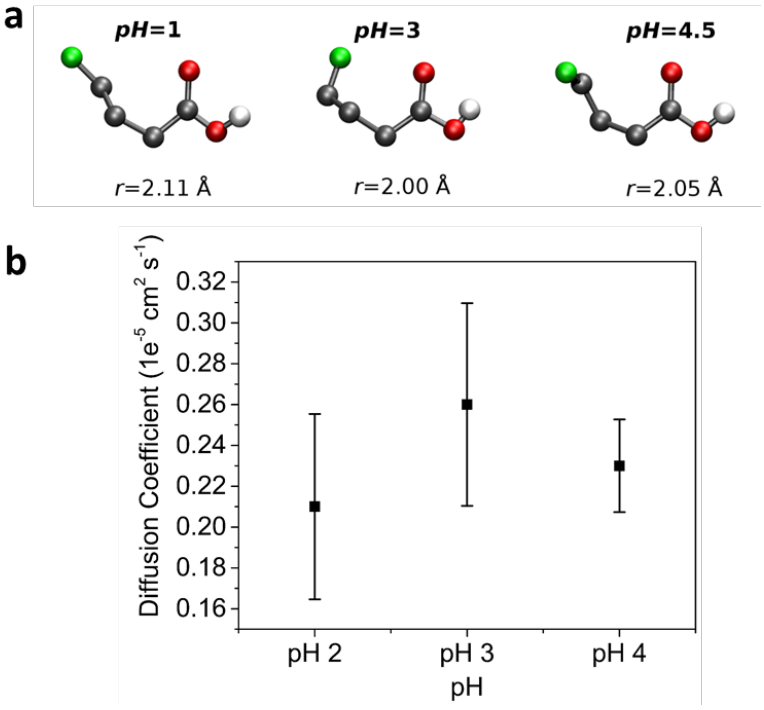

Figure 4. Molecular dynamics results. (a) GABA configurations and radii of gyration. H atoms have been removed for clarity, except from OH groups (C: black; N: green; O: red; H: white). (b) GABA diffusion coefficient vs pH.

CONCLUSIONS

In this work, we address the challenge of finding – and understanding – the role of pH in electrophoretic transport in iontronic devices. Specifically, we investigate optimization of transport of the neurotransmitter GABA through OEIPs while varying the pH in the source reservoir. Electrical measurements and chemical quantification were performed to determine the transport efficiency (ratio of intended-transport-molecule:e^-), and find the optimal balance between efficiency and H^+ delivery. Classical molecular dynamics simulations were also performed to elucidate the role of conformational changes on the mobility of cationic GABA through the OEIP channel. Our results indicate a correlation between the pH in the source electrolyte, the associated conformation (and mobility) of GABA, and the transport efficiency; that is, pH 3 is indicated in all experiments as the ideal source pH for efficient GABA transport. While this investigation was confined to GABA as a test substance, these results provide a useful method of optimization for future OEIP applications. This deeper understanding of the implications of shifting pH in the source solution will enable a broader assortment of "pumpable" signaling or neuromodulatory substances, and thus wider application of OEIP technology in basic research and future therapeutics.

AUTHOR INFORMATION

MB and DTS are shareholders in the small, researcher-controlled intellectual property company OBOE IPR AB (oboeipr.com), which own patents related to this research. The authors declare no additional competing financial interests.

ACKNOWLEDGEMENTS

This work was supported primarily by the EU Seventh Framework Programme under grant agreement 607896, project OrgBIO ITN. Additional funding was provided by the Knut and Alice Wallenberg Foundation (Tail of the Sun project, and Wallenberg Scholar, 2012.0302), and by the Önnesjö Foundation. The computations were performed on resources provided by the Swedish National Infrastructure for Computing at the National Supercomputer Centre at Linköping University. We thank Dr. E. Stavrinidou and Dr. A. Jonsson at Linköping University for fruitful discussions.

SUPPORTING INFORMATION DESCRIPTION

The Supporting Information is available free of charge on the ACS Publications website at DOI: 10.1021/acs.jpclett.XXXX.

Experimental methods: Evaluation of leakage and reverse pumping, Ab-initio Calculations (DFT), Conformation analysis, Correlating charge with pH using FTIR; Figure S1, charge distribution for $GABA^+$ and $GABA^0$; Figure S2, GABA protonation; Table S1, experimental $GABA^+$ and H^+ concentrations; Figure S3, FTIR spectra (PDF).

REFERENCES

(1) Simon, D. T.; Gabrielsson, E. O.; Tybrandt, K.; Berggren, M. Organic Bioelectronics: Bridging the Signaling Gap between Biology and Technology. *Chem. Rev.* **2016**, *116* (21), 13009–13041.

(2) Abidian, M. R.; Martin, D. C. Multifunctional Nanobiomaterials for Neural Interfaces. *Adv. Func. Mater.* **2009**, *19* (4), 573–585.

(3) Jonsson, A.; Inal, S.; Uguz, L.; Williamson, A. J.; Kergoat, L.; Rivnay, J.; Khodagholy, D.; Berggren, M.; Bernard, C.; Malliaras, G. G.; et al. Bioelectronic Neural Pixel: Chemical Stimulation and Electrical Sensing at the Same Site. *P. Natl. Acad. Sci.* **2016**,

113 (34), 9440–9445.

(4) Khodagholy, D.; Doublet, T.; Quilichini, P.; Gurfinkel, M.; Leleux, P.; Ghestem, A.; Ismailova, E.; Hervé, T.; Sanaur, S.; Bernard, C.; et al. In Vivo Recordings of Brain Activity Using Organic Transistors. *Nat. Commun.* **2013**, *4*, 1575.

(5) Jonsson, A.; Song, Z.; Nilsson, D.; Meyerson, B. A.; Simon, D. T.; Linderoth, B.; Berggren, M. Therapy Using Implanted Organic Bioelectronics. *Sci. Adv.* **2015**, *1* (4), e1500039.

(6) Isaksson, J.; Kjäll, P.; Nilsson, D.; Robinson, N.; Berggren, M.; Richter-Dahlfors, A. Electronic Control of Ca2+ Signalling in Neuronal Cells Using an Organic Electronic Ion Pump. *Nat. Mater.* **2007**, *6* (9), 673–679.

(7) Simon, D. T.; Kurup, S.; Larsson, K. C.; Hori, R.; Tybrandt, K.; Goiny, M.; Jager, E. W. H.; Berggren, M.; Canlon, B.; Richter-Dahlfors, A. Organic Electronics for Precise Delivery of Neurotransmitters to Modulate Mammalian Sensory Function. *Nat. Mater.* **2009**, *8* (9), 742–746.

(8) Isaksson, J.; Kjall, P.; Nilsson, D.; Robinson, N. D.; Berggren, M.; Richter-Dahlfors, A. Electronic Control of Ca2+ Signalling in Neuronal Cells Using an Organic Electronic Ion Pump. *Nat Mater* **2007**, *6* (9), 673–679.

(9) Tybrandt, K.; Larsson, K. C.; Kurup, S.; Simon, D. T.; Kjäll, P.; Isaksson, J.; Sandberg, M.; Jager, E. W. H.; Richter-Dahlfors, A.; Berggren, M. Translating Electronic Currents to Precise Acetylcholine-Induced Neuronal Signaling Using an Organic Electrophoretic Delivery Device. *Adv. Mater.* **2009**, *21* (44), 4442–4446.

(10) Williamson, A.; Rivnay, J.; Kergoat, L.; Jonsson, A.; Inal, S.; Uguz, I.; Ferro, M.; Ivanov, A.; Sjöström, T. A.; Simon, D. T.; et al. Controlling Epileptiform Activity with Organic Electronic Ion Pumps. *Adv. Mater.* **2015**, *27* (20), 3138–3144.

(11) Poxson, D. J.; Karady, M.; Gabrielsson, R.; Alkattan, A. Y.; Gustavsson, A.; Ljung, K.; Grebe, M.; Simon, D. T.; Berggren, M. Regulating Plant Physiology with Organic Electronics. *Proc. Natl. Acad. Sci.* **2017**, accepted.

(12) Gabrielsson, E. O.; Tybrandt, K.; Berggren, M. Ion Diode Logics for pH Control. *Lab Chip* **2012**, *12* (14), 2507–2513.

(13) Gabrielsson, E. O.; Janson, P.; Tybrandt, K.; Simon, D. T.; Berggren, M. A Four-Diode Full-Wave Ionic Current Rectifier Based on Bipolar Membranes: Overcoming the Limit of Electrode Capacity. *Adv. Mater.* **2014**, *26* (30), 5143–5147.

(14) Tybrandt, K.; Larsson, K. C.; Richter-Dahlfors, A.; Berggren, M. Ion Bipolar Junction Transistors. *P. Natl. Acad. Sci.* **2010**, *107* (22), 9929–9932.

(15) Tybrandt, K.; Forchheimer, R.; Berggren, M. Logic Gates Based on Ion Transistors. *Nat. Commun.* **2012**, *3* (May), 871.

(16) Jonsson, A.; Sjöström, T. A.; Tybrandt, K.; Berggren, M.; Simon, D. T. Chemical Delivery Array with Millisecond Neurotransmitter Release. *Sci. Adv.* **2016**, *2* (11), e1601340–e1601340.

(17) Strathmann, H. *Ion-Exchange Membrane Separation Processes*; Elsevier, 2004.

(18) Strakosas, X.; Wei, B.; Martin, D. C.; Owens, R. M. Biofunctionalization of Polydioxythiophene Derivatives for Biomedical Applications. *J. Mater. Chem. B* **2016**, *4* (29), 4952–4968.

(19) Lin, Y. S.; Li, G. De; Mao, S. P.; Chai, J. Da. Long-Range Corrected Hybrid Density Functionals with Improved Dispersion Corrections. *J. Chem. Theory Comput.* **2013**, *9* (1), 263–272.

(20) Krishnan, R.; Binkley, J. S.; Seeger, R.; Pople, J. A. Self-Consistent Molecular Orbital Methods. XX. A Basis Set for Correlated Wave Functions. *J. Chem. Phys.* **1980**, *72* (1), 650–654.

(21) Singh, U. C.; Kollman, P. A. An Approach to Computing Electrostatic Charges for Molecules. *J. Comput. Chem.* **1984**, *5* (2), 129–145.

(22) Frisch, M. J.; Trucks, G. W.; Schlegel, H. B.; Scuseria, G. E.; Robb, M. A.; Cheeseman, J. R.; Scalmani, G.; Barone, V.; Mennucci, B.; Petersson, G. A.; et al. Gaussian~09 Revision E.01.

(23) Wang, J.; Wolf, R. M.; Caldwell, J. W.; Kollman, P. A.; Case, D. A. Development and Testing of a General Amber Force Field. *J. Comput. Chem.* **2004**, *25* (9), 1157–1174.

(24) Berendsen, H.; Postma, J.; van Gunsteren, W.; Hermans, J. Intermolecular Forces; Pullman, B., Ed.; Reidel, Dordrecht, 1981; pp 331–342.

(25) Review, P.; Shiga, M.; Agency, E. Rapid Estimation of Elastic Constants by Molecular Dynamics Simulation under Constant Stress. **2004**, No. August 2014.

(26) Martyna, G. J.; Tobias, D. J.; Klein, M. L. + E. **1994**, *101* (September), 4177–4189.

(27) Rahman, M. P. Polymorphic Transitions in Single Crystals : A New Molecular Dynamics Method Polymorphic Transitions in Single Crystals : A New Molecular Dynamics Method. **2007**, *7182* (1981).

(28) Plimpton, S. Fast Parallel Algorithms for Short-Range Molecular Dynamics. *Journal of Computational Physics*. 1995, pp 1–19.

(29) Edward, J. T. Molecular Volumes and the Stokes-Einstein Equation. *Jorunal Chem. Educ.* **1970**, *47* (4), 261–270.

(30) B, H.; C, K.; van der Spoel D; E, L. GROMACS 4: Algorithms for Highly Efficient, Load-Balanced, and Scalable Molecular Simulation. *J. Chem. Theory. Comput.* **2008**, *4* (3), 435–447.

(31) Mao, Z.; Ma, L.; T, C. G.; Shen, J. Preformed Microcapsules for Loading and Sustained Release of Ciprofloxacin Hydrochloride. **2005**, *104*, 193–202.

(32) Xue, W.; Cui, T.; Lee, D.; Cui, T.; Sarkar, N.; Ram, M. K. Fabrication and Characterization of Metal – Oxide – Semiconductor Capacitor Based on Layer-by-Layer Self-Assembled.

(33) Li, L.; Ferng, L.; Wei, Y.; Yang, C.; Ji, H. Journal of Colloid and Interface Science Effects of Acidity on the Size of Polyaniline-Poly (Sodium 4-Styrenesulfonate) Composite Particles and the Stability of Corresponding Colloids in Water. *J. Colloid Interface Sci.* **2012**, *381* (1), 11–16.

(34) Ottosson, N.; Pastorczak, M.; van der Post, S. T.; Bakker, H. J. Conformation of the Neurotransmitter Gamma-Aminobutyric Acid in Liquid Water. *Phys. Chem. Chem. Phys.* **2014**, *16* (22), 10433–10437.

(35) C.A.J Appelo. Specific Conductance – How to Calculate the Specific Conductance with PHREEQC. **2010**.